To cite this article: YU R Z, YUAN J P, LI J Y. Adaptive control of large transport ship based on grasshopper optimization algorithm [J/OL]. Chinese Journal of Ship Research, 2023, 18(3). http://www.ship-research.com/en/article/doi/10.19693/j.issn.1673-3185.02782.

DOI: 10.19693/j.issn.1673-3185.02782

Adaptive control of large transport ship based on grasshopper optimization algorithm

YU Rongzhen[1], *YUAN Jianping*[*2], *LI Junyi*[3]

1 College of Electronics and Information Engineering, Guangdong Ocean University, Zhanjiang 524088, China
2 College of Ocean Engineering, Guangdong Ocean University, Zhanjiang 524088, China
3 Wuhan Second Ship Design and Research Institute, Wuhan 430205, China

Abstract: [**Objectives**] The maritime navigation environment is random, complex and changeable, and intelligent autonomous navigation is an important trend in the development of large ocean-going transport ships, for which a new adaptive control method is proposed. [**Methods**] First, the linear quadratic regulator (LQR) control method is integrated with the first-order dynamic integral sliding mode control method based on the grasshopper optimization algorithm (GOA). A nonlinear passive estimator with real-time monitoring of wave disturbance forces is then combined to separate the high and low-frequency motion signals of the ship. Finally, the simulation results of the proposed method are compared with those of the LQR control method and first-order dynamic integral sliding mode control method. [**Results**] The results show that the new control method has better transient and steady-state tracking performance, and is able to overcome the effects of random waves under different sea conditions with strong robustness. [**Conclusions**] The new control method has such abilities as self-adjustment in complex environments, fast control response, high precision and less redundant steering, enabling it to greatly improve the navigation efficiency, safety and stability of large transport ships.

Key words: large transport ship; grasshopper optimization algorithm (GOA); sliding mode control; linear quadratic regulator (LQR); tracking control

CLC number: U675.9; TP273

0 Introduction

As important platforms for ocean transportation, large transport ships navigate in complex and changing marine environments in long cycles at high energy consumption. Safe, energy-saving, and efficient navigation are thus extremely important for such ships[1]. In the field of motion control, ships are long-time-delay systems due to their large displacements and high metacenters and are highly likely to capsize in high sea states. For this reason, motion response is one of the bottlenecks that need to be solved. The development of marine transport ships towards higher performance and higher technologies has become increasingly pronounced amid the application of artificial intelligence, big data, and other kinds of new technologies in the field of marine equipment. Specifically, seeking better transient and steady-state heading tracking performance under constraints and exploring better

Received: 2022－01－19 **Accepted**: 2022－05－06

Supported by: Stability Support Project of State Administration of Science, Technology and Industry for National Defence, PRC (JCKYS2021SXJQR-02); Special Funds Supporting Project of Artificial Intelligence Key Areas in Guangdong General Colleges and Universities (2019KZDZX1024)

Authors: YU Rongzhen, male, born in 1997, master's degree candidate. Research interest: autonomous technology of underwater robots. E-mail: 15913696238@163.com

YUAN Jianping, male, born in 1979, master, associate professor. Research interest: intelligent control technology of marine unmanned equipment. E-mail: yjp_103@163.com

LI Junyi, male, born in 1988, doctoral candidate

***Corresponding author**: YUAN Jianping

adaptive performance with a focus placed on the evolution of control algorithms have become important directions for intelligent autonomous navigation.

The motion control of large transport ships has already been investigated extensively. For example, Zhang et al.[1] proposed a robust control algorithm for the safe navigation of an intelligent transport ship in harsh sea states. Focusing on reducing the rolling and improving the effectiveness of a ship in a high sea state, Jin et al.[2] designed an optimal rudder-roll damping controller based on frequency-division linear quadratic regulation (FDLQR) and achieved fast tracking and response. Borkowski[3] proposed a linear quadratic regulator (LQR)-based adaptive control system to determine the control parameters of a ship in a complex time-varying environment. The results revealed satisfactory control quality. Li et al.[4] designed a backstepping sliding mode controller based on the sliding mode control method and the backstepping method for the trajectory control of large unmanned transport ships exposed to external disturbances. To ensure the vertical position of a ship in a harsh sea state, Lee et al.[5] adopted the adaptive fractional-order sliding mode control (AFOSMC) method to effectively regulate the ship's pitching and thereby achieve the closed-loop stability of the ship's pitch system. The above literature made full use of the advantageous stability margin and response speed of LQR-based control methods[6] and the insensitivity of sliding mode control methods to the uncertainty of system models and external disturbances. In this way, it effectively solved the problems concerning the safety and control stability of ships navigating under external disturbances or extreme operating conditions.

In recent years, research efforts have been devoted to solving the problem of adaptive control in complex time-varying environments. A class of swarm intelligence-based optimization algorithms that simulate the behavioral characteristics of biological groups in nature, such as the dragonfly algorithm[7] (DA), the ant-lion optimization[8] (ALO) algorithm, and the whale optimization algorithm[9] (WOA), have been applied for the automatic optimization of control parameters under different operating conditions. Saremi et al.[10] proposed a swarm intelligence-based grasshopper optimization algorithm in 2017 and applied it to parameter optimization. Boasting a simple structure, a small number of parameters, and great stability, the grasshopper optimization algorithm (GOA) was highly competitive in optimization accuracy and solution speed[11]. Moreover, this algorithm could well balance global and local search processes owing to its unique adaptation mechanism[12]. Weighing the requirements on the safety, energy conservation, and accurate control of a ship comprehensively, the authors draw on the GOA and combine LQR-based control with first-order dynamic integral sliding mode control to develop a new control method, thereby enabling the safe and adaptive navigation of a large transport ship in different sea states.

1 Mathematical motion model of large transport ship

A large transport ship on sea is mainly affected by the marine environment in two ways: The slow motion generated by wind, current, and the second-order wave force causes the ship to slowly drift away from its original position; the high-frequency reciprocation generated by the first-order wave force not only accelerates the wear and tear of the thruster system and the consumption of energy when it is to be controlled but also affects the measurement accuracy of sensors. Therefore, the high-frequency component shall be filtered out. In summary, the system shall not only remove the high-frequency motion component and noise from the information of the sensors but also use the predicted values to achieve accurate control of the low-frequency motion. For this reason, the authors handle the high-frequency motion and low-frequency motion of the ship separately.

1.1 Low-frequency motion model of ship

In low sea states, the influences of the pitching, rolling, and heaving of a large ship on its motion in the horizontal plane are small and thus negligible. Therefore, the motion of the ship can be simplified to plane motion in three degrees of freedom. As shown in Fig. 1, the discussion of a mathematical motion model of a ship usually presupposes the construction of a body-fitted coordinate system xoy with the ship's center of gravity as its origin and an inertial coordinate system $X_0O_0Y_0$. In the figure, $\boldsymbol{V} = [u\ v\ r]$ is the linear and angular velocity vectors of a ship, where u, v, and r are the surging velocity, swaying velocity, and yaw rate in the body-fitted coordinate system, respectively; ψ is the heading

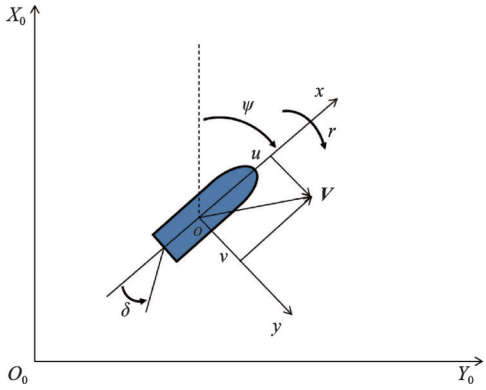

Fig. 1 Relationship between ship's plane body-fitted and inertial coordinate systems

angle; δ is the rudder angle.

The forces on a large transport ship mainly include an inertial hydrodynamic force, a viscous hydrodynamic force, a propeller thrust, a rudder force, and environmental disturbance forces [13]. The standard methods proposed by the research group on mathematical models for ship maneuvering motions can be applied to decouple the dynamical properties in each degree of freedom. In this case, the hydrodynamic equations of each system are physically meaningful [14]. The state variable of a large ship is $\boldsymbol{x} = [u\ v\ r\ x\ y\ \psi]$, and the control input variable of the ship is δ. The nonlinear dynamic equations of the surging, swinging, and yawing of a ship in three-degree-of-freedom plane motion are as follows:

$$\begin{aligned} &m(\dot{u}-vr)+(m_y\dot{u}-m_yvr)= \\ &X_{\mathrm{S}}+(1-t_{\mathrm{p}})\rho n^2D_{\mathrm{p}}^4K_{\mathrm{T}}(J)+(1-t_{\mathrm{R}})F_{\mathrm{N}}\sin\delta+X_{\mathrm{ENV}} \\ &m(\dot{v}+ur)+(m_y\dot{v}+m_xur)=Y_{\mathrm{S}}+(1+a_{\mathrm{H}})F_{\mathrm{N}}\cos\delta+Y_{\mathrm{ENV}} \\ &I_z\dot{r}+J_z\dot{r}=N_{\mathrm{S}}+(x_{\mathrm{R}}+a_{\mathrm{H}}x_{\mathrm{H}})F_{\mathrm{N}}\cos\delta+Z_{\mathrm{ENV}} \end{aligned} \tag{1}$$

where m is the mass of the ship; m_x and m_y are the additional masses on the x and y axes; X_{s}, Y_{s}, and N_{s} are the hydrodynamic equations of the ship's surging, swaying, and yawing, respectively; t_{p} is the thrust deduction factor; t_{R} is the rudder resistance deduction factor; ρ is seawater density; n is the rotational speed of the propeller; D_{p} is the diameter of the propeller; $K_{\mathrm{T}}(J)$ is the thrust coefficient of the propeller, with J being the advance coefficient of the propeller; F_{N} is the positive pressure perpendicular to the rudder blade plane; X_{ENV}, Y_{ENV} and Z_{ENV} are the longitudinal force, transverse force, and rotational moment generated by wind, current, second-order waves, and other environmental disturbances, respectively; a_{H} is the correction factor for the steering-induced transverse force on the hull; I_z is the moment of inertia around the oz axis; J_z is the additional moment of inertia around the z axis; x_{R} is a longitudinal coordinate of the transverse force on the rudder; x_{H} is the distance from the action center of the steering-induced transverse force on the hull to the ship's center of gravity and has a value of about $-0.45L$.

X_{S}, Y_{S}, and N_{S} are expressed as follows, respectively:

$$\begin{aligned} X_{\mathrm{S}} &= X_{(u)}+X_{vv}v^2+X_{vr}vr+X_{rr}r^2 \\ Y_{\mathrm{S}} &= Y_vv+Y_rr+Y_{|v|v}|v|v+Y_{|r|r}|r|r+Y_{vvr}v^2r+Y_{vrr}vr^2 \\ N_{\mathrm{S}} &= N_vv+N_rr+N_{|v|v}|v|v+N_{|r|r}|r|r+N_{vvr}v^2r+N_{vrr}vr^2 \end{aligned} \tag{2}$$

where $X_{(u)}$ is the direct-sailing resistance; Y_vv, Y_rr, N_vv, and N_rr are the linear transverse hydrodynamic forces and the corresponding linear transverse hydrodynamic moments, respectively; $X_{vv}v^2$, $X_{vr}vr$, and $X_{rr}r^2$ are the viscous resistance caused by the ship; $Y_{|v|v}|v|v$, $Y_{|r|r}|r|r$, $Y_{vvr}v^2r$, $Y_{vrr}vr^2$, $N_{|v|v}|v|v$, $N_{|r|r}|r|r$, $N_{vvr}v^2r$, and $N_{vrr}vr^2$ are the nonlinear transverse hydrodynamic forces and the corresponding nonlinear transverse hydrodynamic moments, respectively.

The kinematics and dynamics of the ship in the horizontal plane are modeled as follows:

$$\begin{cases} \dot{u}=\dfrac{(m+m_y)vr+X_{\mathrm{S}}+(1-t_{\mathrm{p}})\rho n^2D_{\mathrm{p}}^4K_{\mathrm{T}}(J)+(1-t_{\mathrm{R}})F_{\mathrm{N}}\sin\delta+X_{\mathrm{ENV}}}{(m+m_x)} \\ \dot{v}=\dfrac{-(m+m_x)ur+Y_{\mathrm{S}}+(1+a_{\mathrm{H}})F_{\mathrm{N}}\cos\delta+Y_{\mathrm{ENV}}}{(m+m_y)} \\ \dot{r}=\dfrac{N_{\mathrm{S}}+(x_{\mathrm{R}}+a_{\mathrm{H}}x_{\mathrm{H}})F_{\mathrm{N}}\cos\delta++Z_{\mathrm{ENV}}}{(I_z+J_z)} \\ \dot{x}=u\cos\psi-v\sin\psi \\ \dot{y}=u\sin\psi+v\cos\psi \\ \dot{\psi}=r \end{cases} \tag{3}$$

1.2 High-frequency motion model of ship

The high-frequency motion of the ship is high-frequency reciprocation generated by the first-order wave force. Saelid et al. [15] introduced a damping term into the wave model to better fit the shape of the Pierson-Moskowitz spectrum. This wave model is expressed as follows:

$$h(s)=\frac{K_\omega s}{s^2+2\lambda\omega_o s+\omega_o^2} \tag{4}$$

where K_ω is the gain constant and $K_\omega = 2\lambda\omega_o I$, with coefficient I describing wave intensity; λ is the relative damping ratio; ω_o is the dominant wave frequency; s is the complex frequency.

Equation (4) is converted into a state-space form to obtain the high-frequency motion model of the ship as

$$\begin{cases}\dot{\xi}_h = \boldsymbol{A}_h\xi_h + \boldsymbol{E}_h\omega_h \\ \eta_h = \boldsymbol{C}_h\xi_h\end{cases} \tag{5}$$

where $\dot{\xi}_h = \left[\dot{\xi}_\psi \ \ \dot{\psi}_h\right]$, with $\dot{\xi}_\psi$, $\dot{\psi}_h$ being the position and speed of the ship in the yawing direction, respectively; ω_h is the zero-mean Gaussian white noise; η_h is the heading angle in the high-frequency motion of the ship; $\boldsymbol{A}_h = \begin{bmatrix} 0 & 1 \\ -\omega_o^2 & -2\lambda\omega_o \end{bmatrix}$; $\boldsymbol{E}_h = \begin{bmatrix} 0 \\ K_\omega \end{bmatrix}$; $\boldsymbol{C}_h = [0 \ \ 1]$.

2 Controller design

LQR-based optimal control is usually used to characterize the optimal solution to a performance metric under several specific constraints and applies to the multi-objective optimization control of systems. Sliding mode control is advantageous in overcoming parameter perturbations and works well on a nonlinear system. Nevertheless, it may be exposed to issues such as control jitter.

In this study, a GOA-based adaptive control system for large transport ships was proposed by combining the advantages of LQR-based optimal control and those of sliding mode control. The control principle is shown in Fig. 2. The outputs of the control system are x, y, and ψ. The input is the instructed heading angle ψ_d. ψ_ω is the change in the heading angle caused by the first-order wave. $\boldsymbol{h}(k)$ is the information vector constituted of the input and output data of the first-order wave model. Specifically, the motion state of a large transport ship was estimated in real time using a nonlinear passive estimator based on the recursive least-squares estimator. Then, the estimated error $\hat{e} = \psi_d - \hat{\psi}$ in heading angle tracking and the estimated yaw rate $\hat{r}$ were used as inputs for adaptive regulation. A GOA-based adaptive controller combining the LQR-based control method with the first-order dynamic integral sliding mode control method was designed. Finally, the instructed rudder angle δ was calculated through adaptive adjustment to enable the estimated tracking error $\hat{e}$ to converge to zero and finally fulfill the heading tracking control of the ship.

The output u_{LQR} of the LQR-based control structure and the one u_{SMC} of the first-order dynamic integral sliding mode control structure were used to obtain the adaptive control parameters of the ship under different operating conditions. For this purpose, the constraints on the ship's safety, energy conservation, and steady-state control accuracy were comprehensively weighed by the GOA for the online adjustment of the position where the optimal solution was obtained [16].

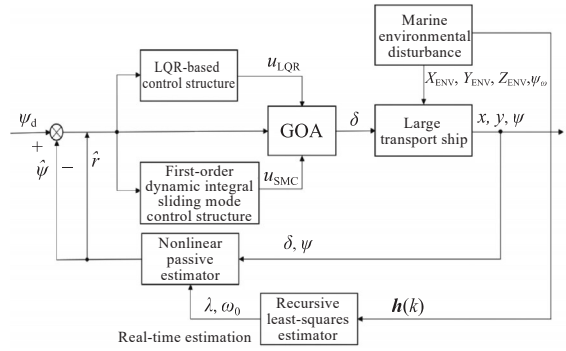

Fig. 2 Principle of motion control of large transport ship

2.1 Estimator

In this study, the recursive least-squares method was combined with a nonlinear passive estimator for online identification of the heading angle and the yaw rate of a ship. As a filtering and state estimation method [17], the nonlinear passive estimator was strongly robust in measuring noise but failed to meet the requirements of high-accuracy system control. Therefore, it needed to be combined with the recursive least-squares method for the online acquirement of the relative damping ratio of the spectrum and the dominant wave frequency it needed. In this way, a more accurate estimator model could be constructed to remove the high-frequency motion components and noise, obtain accurate information on the heading angle and the yaw rate, and ultimately achieve high-accuracy ship motion control.

2.1.1 Nonlinear passive estimator

The nonlinear passive estimator can separate the low-frequency components from the high-frequency components of the horizontal motion of a ship under wave forces, filter out the high-frequency motion caused by first-order waves, and estimate the low-frequency motion state of the ship so that the large transport ship can reach the desired

heading angle more accurately.

The estimator is modeled as follows:

$$\begin{aligned}
\dot{\hat{\xi}}_\omega &= \hat{\psi}_\omega + K_1\left(\psi-\hat{\psi}\right)\\
\dot{\hat{\psi}}_\omega &= -\omega_0^2\hat{\xi}_\omega - 2\lambda\omega_0\hat{\psi}_\omega + K_2\left(\psi-\hat{\psi}\right)\\
\dot{\hat{\psi}} &= \hat{r} + K_3\left(\psi-\hat{\psi}\right)\\
\dot{\hat{r}} &= -\frac{1}{T}\hat{r} + \frac{K}{T}\hat{b} + K_4\left(\psi-\hat{\psi}\right)\\
\dot{\hat{b}} &= -\frac{1}{T_b}\hat{b} + K_5\left(\psi-\hat{\psi}\right)
\end{aligned} \tag{6}$$

where ξ_ω is the sum of multiple harmonic components; K_1, K_2, K_3, K_4, and K_5 are observed gains; T and K are the Nomoto time constant and the Nomoto gain, respectively; b is a disturbance force at a low frequency; Tb is a time constant concerning the rudder offset.

2.1.2 Recursive least-squares estimator

A recursive least-squares estimator was used for real-time observation of the relative damping ratio of the spectrum and the dominant wave frequency the nonlinear passive estimator needed. The basic idea of the least-squares method is as follows: The model is transformed in the form of a Z-transformation (Eq. (7)) of the wave model (Eq. (4)); then, the parameters at the current moment shown in Eq. (8) are estimated using the mathematical model (Eq. (9)) of the recursive least-squares estimator; furthermore, an S-transformation of Eq. (8) is performed to obtain an online wave estimation model; finally, the information observed in real time on the relative damping ratio of the spectrum and the dominant wave frequency is sent to the nonlinear passive estimator to obtain the real-time values of the observed gains to enable the estimator model to be more accurate and real-time.

Equation (4) is discretized into a least-squares regression model:

$$z(k) = \boldsymbol{h}^{\mathrm{T}}(k)\boldsymbol{\theta} \tag{7}$$

where $z(k)$ is the output vector of the system; $\boldsymbol{\theta} = [a_1\ a_2\ a_3\ a_4]$ is the model's parameter vector to be estimated.

In the case of a general discrete nonlinear time-varying system, Eq. (7) can be expressed as

$$z(k) = a_1\boldsymbol{u}(k-1) + a_2\boldsymbol{u}(k-2) + a_3 z(k-1) + a_4 z(k-2) \tag{8}$$

where $\boldsymbol{u}(k)$ is the input vector of the system.

The recursive equations of the least-squares method are as follows:

$$\begin{aligned}
\hat{\boldsymbol{\theta}}(k) &= \hat{\boldsymbol{\theta}}(k-1) + \boldsymbol{K}(k)[z(k) - \boldsymbol{h}^{\mathrm{T}}(k)\hat{\boldsymbol{\theta}}(k-1)]\\
\boldsymbol{K}(k) &= \boldsymbol{P}(k-1)\boldsymbol{h}(k)[\boldsymbol{h}^{\mathrm{T}}(k)\boldsymbol{P}(k-1)\boldsymbol{h}(k)+1]^{-1}\\
\boldsymbol{P}(k) &= [\boldsymbol{I} - \boldsymbol{K}(k)\boldsymbol{h}^{\mathrm{T}}(k)]\boldsymbol{P}(k-1)
\end{aligned} \tag{9}$$

where $\boldsymbol{K}(k)$ is the gain matrix; $\boldsymbol{P}(k)$ is the covariance matrix; $\boldsymbol{I}$ is the unit matrix.

2.2 LQR-based optimal control

State-space equations are presented as follows for the heading control system of a large transport ship:

$$\begin{aligned}
\dot{\boldsymbol{x}}_{\mathrm{L}} &= \boldsymbol{A}\boldsymbol{x}_{\mathrm{L}} + \boldsymbol{B}u_{\mathrm{LQR}}\\
y_{\mathrm{L}} &= \boldsymbol{C}\boldsymbol{x}_{\mathrm{L}}
\end{aligned} \tag{10}$$

where $\boldsymbol{x}_{\mathrm{L}} = [\psi r]^{\mathrm{T}}$ is the state vector; u_{LQR} is the control variable; y_{L} is the output of the system; $\boldsymbol{A}$, $\boldsymbol{B}$, and $\boldsymbol{C}$ in the system shall all be controllable matrices.

The state-space model was investigated to design an LQR to the effect that the controller could track the desired output y_{d} and the error $e=y_{\mathrm{L}}-y_{\mathrm{d}}$ could be reduced to zero. Also, the quadratic objective function J was set to its minimum to obtain the optimal u_{LQR}.

$$J = \frac{1}{2}\int_0^{\mathrm{T}}\left(e^{\mathrm{T}}\boldsymbol{Q}e + u_{\mathrm{LQR}}^{\mathrm{T}}\boldsymbol{R}u_{\mathrm{LQR}}\right)\mathrm{d}t \tag{11}$$

where $\boldsymbol{Q} = \boldsymbol{Q}^{\mathrm{T}} > 0$, $\boldsymbol{R} = \boldsymbol{R}^{\mathrm{T}} > 0$ are the positive semi-definite state weighting matrix and the positive definite control weighting matrix, respectively, and are usually set to two diagonal matrices. The LQR-based optimal control law obtained is as follows:

$$u_{\mathrm{LQR}} = -\boldsymbol{R}^{-1}\boldsymbol{B}^{\mathrm{T}}\boldsymbol{P}\boldsymbol{x}_{\mathrm{L}} \tag{12}$$

where $\boldsymbol{P}$ is the positive definite real symmetric square matrix that is also a solution satisfying the Riccati algebraic equation $\boldsymbol{PA} + \boldsymbol{A}^{\mathrm{T}}\boldsymbol{P} - \boldsymbol{PBR}^{-1}\boldsymbol{B}^{\mathrm{T}}\boldsymbol{P} = -\boldsymbol{Q}$.

The Lyapunov function is considered:

$$V_{\mathrm{LQR}} = \boldsymbol{x}_{\mathrm{L}}^{\mathrm{T}}\boldsymbol{P}\boldsymbol{x}_{\mathrm{L}} \tag{13}$$

$u_{\mathrm{LQR}}=\boldsymbol{K}\boldsymbol{x}_{\mathrm{L}}$ is selected as the output, with the optimal feedback coefficient matrix $\boldsymbol{K} = -\boldsymbol{R}^{-1}\boldsymbol{B}^{\mathrm{T}}\boldsymbol{P}$.

The derivative of V_{LQR} is obtained:

$$\begin{aligned}
\dot{V}_{\mathrm{LQR}} &= \dot{\boldsymbol{x}}_{\mathrm{L}}^{\mathrm{T}}\boldsymbol{P}\boldsymbol{x}_{\mathrm{L}} + \boldsymbol{x}_{\mathrm{L}}^{\mathrm{T}}\boldsymbol{P}\dot{\boldsymbol{x}}_{\mathrm{L}} =\\
&\boldsymbol{x}_{\mathrm{L}}^{\mathrm{T}}(\boldsymbol{A}^{\mathrm{T}} - \boldsymbol{K}^{\mathrm{T}}\boldsymbol{B}^{\mathrm{T}})\boldsymbol{P}\boldsymbol{x}_{\mathrm{L}} + \boldsymbol{x}_{\mathrm{L}}^{\mathrm{T}}\boldsymbol{P}(\boldsymbol{A} - \boldsymbol{BK})\boldsymbol{x}_{\mathrm{L}} =\\
&\boldsymbol{x}_{\mathrm{L}}^{\mathrm{T}}(\boldsymbol{A}^{\mathrm{T}}\boldsymbol{P} + \boldsymbol{PA} - \boldsymbol{K}^{\mathrm{T}}\boldsymbol{B}^{\mathrm{T}}\boldsymbol{P} - \boldsymbol{PBK})\boldsymbol{x}_{\mathrm{L}} =\\
&\boldsymbol{x}_{\mathrm{L}}^{\mathrm{T}}(-\boldsymbol{Q} + \boldsymbol{PBR}^{-1}\boldsymbol{B}^{\mathrm{T}}\boldsymbol{P} - \boldsymbol{K}^{\mathrm{T}}\boldsymbol{B}^{\mathrm{T}}\boldsymbol{P} - \boldsymbol{PBK})\boldsymbol{x}_{\mathrm{L}} =\\
&\boldsymbol{x}_{\mathrm{L}}^{\mathrm{T}}(-\boldsymbol{Q} + \boldsymbol{PB}(\boldsymbol{R}^{-1} - \boldsymbol{R}^{-1} - \boldsymbol{R}^{-1})\boldsymbol{B}^{\mathrm{T}}\boldsymbol{P})\boldsymbol{x}_{\mathrm{L}} =\\
&\boldsymbol{x}_{\mathrm{L}}^{\mathrm{T}}(-\boldsymbol{Q} - \boldsymbol{PBR}^{-1}\boldsymbol{B}^{\mathrm{T}}\boldsymbol{P})\boldsymbol{x}_{\mathrm{L}}
\end{aligned} \tag{14}$$

Equation (14) suggests that $\dot{V}_{\mathrm{LQR}}<0$. In this case, the closed-loop system is stable.

2.3 First-order dynamic integral sliding mode control

Sliding mode control is insensitive to perturbations and can overcome parameter perturbations. For this reason, it works well on a large transport ship operating in complex

environments as it enables the system to be sufficiently robust. Integral sliding mode control can eliminate the steady-state error and obtain satisfactory transient performance, while first-order dynamic sliding mode control can be developed to solve the "buffeting" problem. Therefore, the authors explore a control method based on first-order dynamic integral sliding mode control for large transport ships.

A state-space equation is established as follows for the heading control system of a large transport ship:

$$\begin{bmatrix} \dot{\psi} \\ \dot{r} \end{bmatrix} = \begin{bmatrix} 0 & 1 \\ 0 & \dfrac{N_r}{I_z - N_{\dot{r}}} \end{bmatrix} \begin{bmatrix} \psi \\ r \end{bmatrix} + \begin{bmatrix} 0 \\ \dfrac{-N_\delta}{I_z - N_{\dot{r}}} \end{bmatrix} u_{\mathrm{SMC}} \quad (15)$$

where N_r, N_δ, and $N_{\dot{r}}$ are hydrodynamic coefficients.

For a smaller steady-state error, a term containing the integral of the tracking error is added into the conventional sliding mode surface to obtain the integral sliding mode surface s_{I}

$$s_{\mathrm{I}} = \dot{e} + k_{\mathrm{P}} e + k_{\mathrm{I}} \int_0^t e(t)\mathrm{d}t \quad (16)$$

where e is the tracking error and $e = \psi - \psi_{\mathrm{d}}$; $k_{\mathrm{P}} > 0$; $k_{\mathrm{I}} > 0$.

The system state traverses back and forth between the two sides of the sliding mode surface once the system state reaches the sliding surface, and the control variable constantly jitters. This is the main obstacle restraining the practical application of sliding mode control. For effectively reduced "buffeting" and the achievement of the desired performance, first-order dynamic sliding mode control is developed to transfer the discontinuous term in the control input into the first-order derivative of the control input and thereby obtain a control input continuous in time[18].

The first-order derivative of the sliding mode surface is

$$\dot{s}_{\mathrm{I}} = \dot{r} + k_{\mathrm{P}} r + k_{\mathrm{I}} e \quad (17)$$

Then, s is taken as the system state to construct a new dynamic switching function

$$\sigma = \dot{s}_{\mathrm{I}} + \lambda_{\mathrm{I}} s_{\mathrm{I}} \quad (18)$$

where $\lambda_{\mathrm{I}} > 0$. The derivative of σ is obtained as follows:

$$\dot{\sigma} = \ddot{s}_{\mathrm{I}} + \lambda_{\mathrm{I}} \dot{s}_{\mathrm{I}} \quad (19)$$

The Lyapunov function is defined as

$$V_{\mathrm{SMC}} = \frac{1}{2}\sigma^2 \quad (20)$$

The exponential reaching law is selected to accelerate the reaching process, reduce the "buffeting", and ultimately enable the system to reach σ in a finite time regardless of its initial state. The reaching law is as follows:

$$\dot{\sigma} = -\varepsilon \mathrm{sgn}(\sigma) - k\sigma \quad (21)$$

where ε and k are both positive constants; sgn(x) is a sign function.

The derivative of Eq. (20) is obtained

$$\dot{V}_{\mathrm{SMC}} = \sigma\dot{\sigma} = -\sigma\varepsilon \mathrm{sgn}(\sigma) - k\sigma^2 = -\varepsilon|\sigma| - k\sigma^2 < 0 \quad (22)$$

According to Eqs. (15) to (21), a dynamic integral control law can be obtained as

$$\dot{u}_{\mathrm{SMC}} = \left[-\varepsilon \mathrm{sgn}(\sigma) - k\sigma - \lambda_{\mathrm{I}}(\dot{r} + k_{\mathrm{P}} r + k_{\mathrm{I}} e) - k_{\mathrm{P}}\dot{r} - k_{\mathrm{I}} r - \frac{N_r}{I_z - N_{\dot{r}}}\dot{r} \right] / \frac{-N_\delta}{I_z - N_{\dot{r}}} \quad (23)$$

Equation (22) indicates that the function V_{SMC} satisfies the criterion of the Lyapunov function. When the motion is normal and far from the switching surface, it can reach the switching surface quickly and then stabilize. When the motion is close to the switching surface $\sigma = 0$, $\dot{s}_{\mathrm{I}} + \lambda_{\mathrm{I}} s_{\mathrm{I}} = 0$, and the system is an asymptotically stable first-order dynamic system with an s_{I} tending to zero. As a result, the robustness and convergence of the system are ensured.

2.4 GOA iteration model

The GOA is a new swarm intelligence-based optimization algorithm proposed in recent years. Simulating the foraging behavior of grasshoppers in nature, it is a mathematical model that can simulate the repulsive and attractive forces among grasshoppers. In this study, the interaction among individuals in the GOA is utilized to combine LQR-based control with first-order dynamic integral sliding mode control. Then, a GOA-based control method for large transport ships is investigated with due consideration given to multi-objective requirements, such as environmental adaptation, ship safety, and transient and steady-state tracking performance, for hybrid optimization of control parameter selection and outputs. In the GOA, the next position of grasshopper iteration is updated according to grasshoppers' current and optimal positions. The position update model for grasshoppers is as follows:

$$X = c\left(c\frac{b_{\mathrm{u}} - b_{\mathrm{l}}}{2} g\left(\left|u_{\mathrm{LQR}} - u_{\mathrm{SMC}}\right|\right) \frac{u_{\mathrm{LQR}} - u_{\mathrm{SMC}}}{d} \right) + T_{\mathrm{d}} \quad (24)$$

where c is the decreasing coefficient, a parameter determining the sizes of the comfort zone, the repulsion region, and the attraction region, and the c inside the equation helps reduce the repulsive or attractive force among grasshoppers while the one

outside the equation can reduce the search areas around the target as the number of iterations rises; $g(d)$ is the social influence whose negative value indicates mutual repulsion and whose positive value suggests mutual attraction, and it is calculated by Eq. (25); b_u and b_l are the upper and lower bounds of $g(d)$, respectively. $d = \left|u_{LQR} - u_{SMC}\right|$ is the distance among grasshoppers; T_d is the optimal position.

$$g(d) = f\mathrm{e}^{\frac{-d}{l}} - \mathrm{e}^{-d} \tag{25}$$

where f is the attraction intensity among grasshoppers; l is the range of the attraction among grasshoppers. The repulsive force among grasshoppers contributes to their global search while the attraction among them ensures that they find the target location of food.

The parameter c is updated using Eq. (26). The global search is reduced while the precise local search is increased as the number of iterations rises. The calculation equation is as follows:

$$c = c_{max} - L_n \frac{c_{max} - c_{min}}{L} \tag{26}$$

where c_{max} and c_{min} are the maximum and minimum of c, respectively; L_n is the current number of iterations; L is the maximum number of iterations. In the whole search process, the quality of the grasshopper location is judged by the fitness function $D=\psi-\psi_d$. The optimal solution is obtained by continuously cycling iterations. The value calculated using the fitness function is fitness, and the optimal fitness obtained by iterations is considered the value of the optimal solution obtained so far. The location of the optimal solution obtained is the current target location T_d of the food [19].

3 Simulation analysis

To verify the correctness and effectiveness of the proposed control method, the authors take COSCO SHANGHAI shown in Fig. 3 as the object of simulation tests. With a cargo capacity of 5 618 TEU, this ship is a Panamax container ship, and its main dimensions are as follows: a length of 280 m, a width of 39.8 m, a molded depth of 23.6 m, a displacement of 69 500 t, an average draft of 7.2 m; a rudder aspect ratio of 1.082, and a hard-over angle of 20°. In the simulation, the state variable $\boldsymbol{x} = [u\ v\ r\ x\ y\ \psi]$ of a large ship has the following initial value: $u_0 = 6$ m/s; $v_0 = 0$; $r_0 = 0$; $x_0 = 0$; $y_0 = 0$; $\psi_0 = 0$. In sea state 3, the significant wave height H_s is 1.2 m; the wave intensity factor I in high-frequency motion is 0.4 m; the relative damping ratio $\lambda = 0.26$; the dominant wave frequency $w_0 = 0.9$ rad/s; the cut-off frequency of the nonlinear passive estimator is 1.0 rad/s. In sea state 5, $H_s = 3.0$ m; $I = 0.9$ m; $\lambda = 0.26$; $w_0 = 0.6$ rad/s; the cut-off frequency of the nonlinear passive estimator is 0.7 rad/s.

Fig. 3 Large transport ship COSCO SHANGHAI [20]

3.1 Comparative analysis of three control methods under class 3 sea state

Fig. 4 shows the curves of the heading angle tracking of a large transport ship model adopting three control methods, namely, LQR-based control, first-order dynamic integral sliding mode control, and GOA-based control, in sea state 3. According to the figure, the curve of the heading angle instruction is a segmented straight line. The large transport ship can automatically travel along the predetermined heading direction, and the actual heading angle curve, smooth and oscillation-free, is close to the required straight line. The ship can be prevented from yawing by improving the accuracy of tracking error control to promote the safety and reliability of ship navigation.

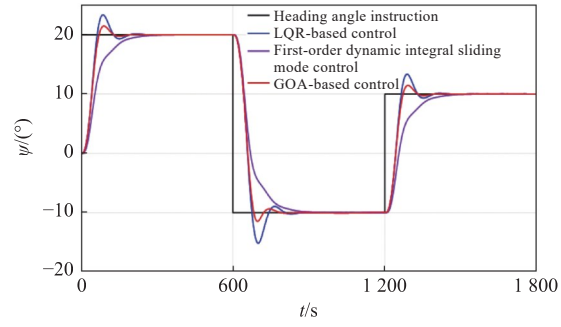

Fig. 4 Curves of heading angle tracking

The comparison between the LQR-based control method and the first-order dynamic integral sliding mode control method shown in Table 1 reveals that the LQR-based control system has an adjustment time of 158.4 s and no steady-state error. This control method provides a faster response speed and a smaller steady-state error. However, it has an overshoot of 33.48%, which is large. In contrast, the first-order dynamic integral sliding mode

Table 1 Response indexes of large transport ship adopting three control methods in three stages

Control method	Response indexes			
	Average steady-state error/(°)	Average adjustment time/s	Average overshoot/%	Number of steering
LQR-based control	–	158.4	33.48	193
First-order dynamic integral sliding mode control	0.1	202.7	2.12	163
GOA-based control	–	127.1	12.16	164

Note: The average steady-state error, average adjustment time, and average overshoot are obtained by arithmetically averaging the steady-state error, adjustment time, and overshoot of three stages in 1 800 s, respectively.

control system is robust with a steady-state error of 0.1° and an overshoot of 2.12%. Nevertheless, its response speed is slow with an adjustment time of 202.7 s. According to the GOA-based control curve shown in Fig. 4 and the data in Table 1, the GOA-based control method has the advantages of both the LQR-based control method and the first-order dynamic integral sliding mode control method. Specifically, this control system, with an adjustment time of 127.1 s, has a faster response speed and an overshoot of 12.16%. Moreover, it has a smooth control curve and no steady-state error, indicating a fair control effect. This control method not only has the characteristic small overshoot and strong robustness of the first-order dynamic integral sliding mode control method but also responds faster than the LQR-based control method and offers the advantage of no steady-state error. As a result, the large transport ship achieves a proper balance between the requirements of robustness and high heading tracking accuracy under external disturbances, which suggests that the GOA-based control method can serve as a theoretical reference to some extent.

When the ship deviates from its original heading by a particular angle due to the action of external forces, the rudder angle can correct the ship's yaw in time to render the heading close to the required straight line. Fig. 5 shows the curves of the rudder angle response of the large transport ship model controlled by three methods in sea state 3. As can be seen from Table 1, the number of steering is 193 for the LQR-based control method and 164 for the GOA-based control method, which is 15% smaller than the former. In this way, the GOA-based control method ensures the ship's safe navigation and reduced energy consumption. In general, the GOA-based control method is relatively superior in multiple aspects, such as stability, economy, and transient and steady-state tracking performance.

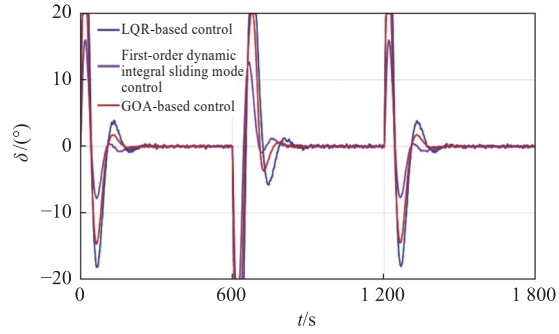

Fig. 5 Curves of rudder angle response

3.2 Analysis of results of GOA-based control method in different sea states

Fig. 6 shows the curves of the predicted yaw-inducing wave disturbance. As can be seen from the figure, the large ship is affected by the disturbance considerably during navigation. In sea state 3, the maximum actual noise ψ_ω is 0.3° and the maximum predicted noise $\hat{\psi}_\omega$ is 0.52°. In sea state 5, the maximum ψ_ω is 1.39° and the maximum $\hat{\psi}_\omega$ is 1.23°. The average predicted noise is nearly zero in both cases, indicating that the nonlinear passive estimator based on the recursive least-squares estimator can estimate the ambient noise induced by the first-order wave force accurately. This estimator can effectively filter out the high-frequency components caused by first-order waves and estimate the heading angle state of the ship, thereby avoiding frequent steering, which is important for reducing rudder wear and tear and energy consumption[21].

Fig. 7 and 8 compare the simulation results of the GOA-based control method in sea states 5 and 3 and in the case of no wind and wave disturbances. As can be seen from Fig. 7, the ship's curve of actual heading angle tracking in sea state 3 almost coincides with the curve in the case of no wind and wave disturbances. It indicates that the GOA-based control method enables the large transport ship to achieve stable navigation under disturbances in sea state 3. In sea state 5, the overshoot and adjustment

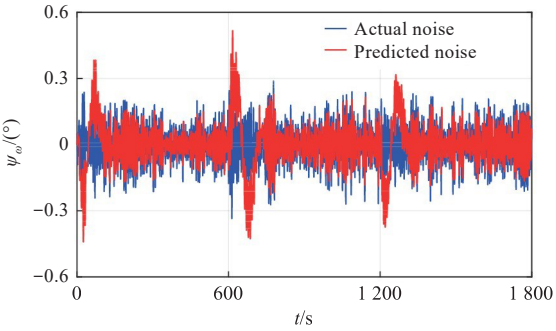

(a) Sea state 3

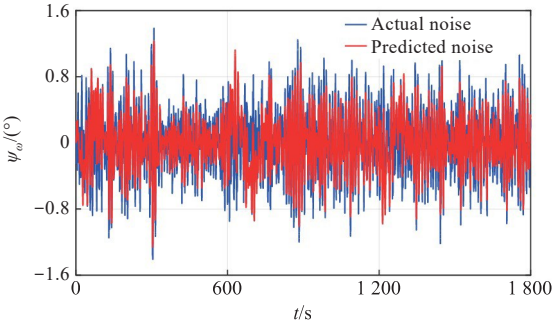

(b) Sea state 5

Fig. 6 Curves of predicted yaw-inducing wave disturbance

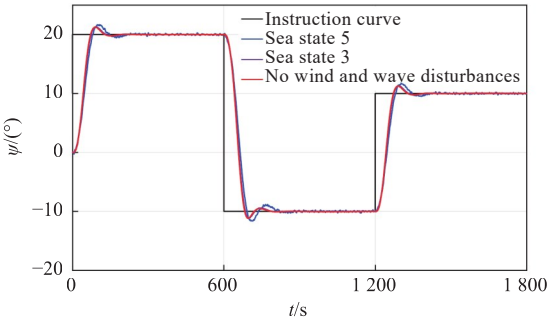

Fig. 7 Curves of heading angle tracking of large transport ship adopting GOA-based control method in different sea states

time of the curve of actual heading angle tracking when the ship adopts the GOA-based control method increase from 12.16% and 127.1 s in sea state 3 to 16.47% and 151.67 s, respectively. Neither the overshoot nor the adjustment time changes significantly. No steady-state error is observed in sea state 5, and the control performance remains satisfactory. In these two sea states, the ship's heading is well controlled by the controller. In summary, the GOA-based control method is readily applicable to the operation of intelligent ships exposed to external disturbances owing to its strong robustness, high-accuracy control performance, and capability to overcome the influence of random waves.

According to Fig. 8, the number of steering for a large transport ship adopting the GOA-based control method is 164 in sea state 3 and 181 in sea state 5. Clearly, it does not change much as the operating condition changes from sea state 3 to sea state 5, indicating favorable control performance. The steering frequency output by the controller is low in both sea states, which suggests that the GOA-based control method can reduce the frequent steering of a ship and is thus economical.

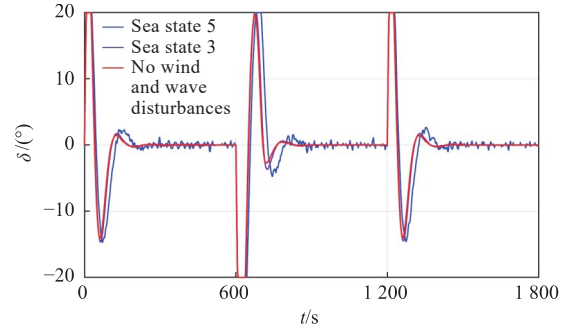

Fig. 8 Curves of rudder angle response of large transport ship adopting GOA-based control method in different sea states

4 Conclusion

A GOA-based adaptive control method for large transport ships was proposed in this study. The motion state of a large transport ship was estimated in real time by adding a nonlinear passive estimator based on a recursive least-squares estimator to feedback control. This measure effectively reduced the number of frequent steering, lowered energy consumption, and improved the robustness and economy of the large transport ship. The simulation results show that the GOA-based adaptive control method for large transport ships combines the advantages of the LQR-based control method with those of the first-order dynamic integral sliding mode control method in the closed-loop simulated system. In this way, the GOA-based control method achieves better transient and steady-state tracking performance and strong robustness, can adjust parameters online, and enhances the adaptive property of the controller. This control method can overcome the influence of random waves and offer strong robustness in different sea states, ultimately reducing the number of frequent steering of a ship. Clearly, the GOA-based control method can substantially improve the safety, stability, and control accuracy of a large transport ship during navigation, and it is thus an effective and feasible control method.

References

[1] ZHANG X K, HAN X. The motion control strategy for

intelligent ships based on ship transportation safeguard [J]. Chinese Journal of Ship Research, 2019, 14(Supp 1): 1−6 (in Chinese).
[2] JIN Z J, SI C S, QIU G Y, et al. Research on course and roll control of ship using jet rudder based on FDLQR [J]. Ship Science and Technology, 2020, 42 (15): 74−81 (in Chinese).
[3] BORKOWSKI P. Adaptive system for steering a ship along the desired route [J]. Mathematics, 2018, 6(10): 196.
[4] LI M C, GUO C, YUAN Y. Adaptive backstepping sliding mode control for straight line track of unmanned transport ship [J]. Journal of System Simulation, 2018, 30(11): 4448−4453, 4461 (in Chinese).
[5] LEE S D, YOU S S, XU X, et al. Active control synthesis of nonlinear pitch-roll motions for marine vessels [J]. Ocean Engineering, 2021, 221: 108537.
[6] WEI M J, WANG C Q, XU C. Research on heading statically unstable aircraft control method based on improved LQR [J]. Control and Information Technology, 2019(4): 85−90 (in Chinese).
[7] MIRJALILI S. Dragonfly algorithm: a new meta-heuristic optimization technique for solving single-objective, discrete, and multi-objective problems [J]. Neural Computing and Applications, 2016, 27(4): 1053−1073.
[8] MIRJALILI S. The ant lion optimizer [J]. Advances in Engineering Software, 2015, 83: 80−98.
[9] HAO X H, SONG J X, ZHOU Q, et al. Improved whale optimization algorithm based on hybrid strategy [J]. Application Research of Computers, 2020, 37(12): 3622−3626, 3655 (in Chinese).
[10] SAREMI S, MIRJALILI S, LEWIS A. Grasshopper optimisation algorithm: theory and application [J]. Advances in Engineering Software, 2017, 105: 30−47.
[11] MIRJALILI S Z, MIRJALILI S, SAREMI S, et al. Grasshopper optimization algorithm for multi-objective optimization problems [J]. Applied Intelligence, 2018,48(4): 805−820.
[12] CHENG Z X, LI D S, GAO Y. UAV three-dimensional path planning based on the grasshopper algorithm [J]. Flight Dynamics, 2019, 37(2): 46−50, 55 (in Chinese).
[13] WU Y, YANG S Q, LI W H, et al. Heading control of an underactuated unmanned surface vehicle based on sliding mode and backstepping [J]. Science Technology and Engineering, 2018, 18(1): 47−53 (in Chinese).
[14] RU Z J. Application of MMG separation modeling in the development process of ship maneuverability simulation software [J]. Ship Science and Technology, 2020, 42(22): 172−174 (in Chinese).
[15] SAELID S, JENSSEN N, BALCHEN J. Design and analysis of a dynamic positioning system based on Kalman filtering and optimal control [J]. IEEE Transactions on Automatic Control, 1983, 28(3): 331−339.
[16] SHEN Z P, DAI C S, ZHANG N. Trajectory tracking control of underactuated ship based on adaptive iterative sliding mode [J]. Journal of Traffic and Transportation Engineering, 2017, 17(6): 125−134 (in Chinese).
[17] FOSSEN T I. Handbook of marine craft hydrodynamics and Motion Control[M]. Hoboken: Wiley, 2011.
[18] LIU J K. Sliding mode control design and MATLAB simulation [M]. 2nd ed. Beijing: Tsinghua University Press,2012 (in Chinese).
[19] ZHAO R, GUO Z C, ZHU X Y. An improved grasshopper optimization algorithm based on levy flight [J]. Computer and Modernization, 2020(1): 104−110 (in Chinese).
[20] Vessel Finder. COSCO SHANGHAI [EB/OL]. (2014-11-13) [2022-12-19]. https: //www. vesselfinder. com/shipphotos/75862.
[21] QIN Z H, LIN Z, LI P, et al. Sliding-mode control of underactuated ship based on LOS guidance [J]. Journal of Central South University (Science and Technology), 2016, 47(10): 3605−3611 (in Chinese).

基于蝗虫优化算法的大型运输船舶自适应控制

余荣臻[1],袁剑平[*2],李俊益[3]
1 广东海洋大学 电子与信息工程学院,广东 湛江 524088
2 广东海洋大学 海洋工程学院,广东 湛江 524088
3 武汉第二船舶设计研究所,湖北 武汉 430205

摘　要:[**目的**]海上航行环境随机复杂多变,而智能自主航行是大型远洋运输船舶发展的重要趋势,为此,提出一种新的自适应控制方法。[**方法**]首先,基于蝗虫优化算法(GOA),将线性二次型调节器(LQR)控制方法与一阶动态积分滑模控制方法相融合;然后,结合实时监测波浪干扰力的非线性无源估计器,将船舶高、低频运动信号进行分离;最后,与LQR 控制方法和一阶动态积分滑模控制方法进行仿真对比。[**结果**]结果显示,新的控制方法具有更好的瞬态和稳态跟踪性能,在不同的海况下能够克服随机波浪的影响,具有较强的鲁棒性。[**结论**]新的控制方法具有复杂环境下的自适应调节能力,且控制响应快、精度高、无效操舵少,能极大地提高大型运输船舶的航行效率、安全性和稳定性。

关键词:大型运输船舶;蝗虫优化算法;滑模控制;线性二次型调节器;跟踪控制